Dalton Transactions

PAPER

View Article Online
View Journal | View Issue

Cite this: *Dalton Trans.*, 2019, **48**, 15928

A single-ion single-electron cerrous magnet†‡

Sandeep K. Gupta, [a] Swaminathan Shanmugan, [a,b] Thayalan Rajeshkumar,[a] Aditya Borah,[a] Marko Damjanović,[c] Michael Schulze,[c] Wolfgang Wernsdorfer, [c] Gopalan Rajaraman *[a] and Ramaswamy Murugavel *[a]

Received 25th July 2019,
Accepted 21st August 2019

DOI: 10.1039/c9dt03052b

rsc.li/dalton

Herein, we present monometallic Ln(III) complexes $[L_3Ln(NO_3)_3]$ [where Ln = Ce (**1**) and La (**2**)] assembled from a simple reaction of the respective lanthanide nitrate hydrate and a bulky phosphonic diamide $^tBuPO(NH^iPr)_2$ ligand (**L**), where complex **1** behaves as a single-ion single-electron magnet under a small applied magnetic field. The Ce(III) ion occupies a nine-coordinate distorted muffin-like coordination environment. The combination of direct and Raman process dominates the relaxation dynamics in **1** under the applied dc field. The low-temperature measurements performed with oriented crystals on a micro-SQUID setup exhibits strong tunnelling at zero-field, consistent with the theoretical results where strong mixing of the ground state with higher excited m_J levels is detected and also throws additional insights on the relaxation dynamics of **1**. *Ab initio* calculations have been performed to understand the origin of anisotropy and models have been proposed for future directions.

Introduction

Incredible growth in the area of single-molecule magnets (SMMs) has been observed in the last two decades; they show a classical magnet-like behaviour along with quantum phenomena such as quantum tunnelling of magnetization (QTM) and quantum coherence in the molecular regime, which have been driven by their potential futuristic applications in developing high-density memory devices, molecular spintronics, and qubits.[1] The report on the phthalocyaninato-based double-decker Tb(III) complex $[Pc_2Tb]^-[TBA]^+$, a single-ion magnet (SIM), acted as a trigger that led material chemists to develop 4f-ion-based SMMs with high anisotropic energy barriers.[2] Since then, the field has seen exponential growth with a major thrust in developing 4f-SMMs, particularly based on heavier ions such as Dy(III), Tb(III) and Er(III) because of their inherent large single-ion anisotropy and large ground m_j quantum states.[3] Apart from the single-ion anisotropy, the crystal field (CF) environment and its interaction, albeit weak, with the f-electronic charge distribution (prolate or oblate) plays a vital role in determining the resultant magnetic anisotropy of any SIM.[4]

Nonetheless, while most of the reported SMMs with remarkable magnetic features reported in the literature are based on the above three heavier 4f ions, the classical hard magnets employed in the industry are based on lighter 4f ions (such as $SmCo_5$ and $Nd_2Fe_{14}B$).[5] Recently, it was reported that Ce(III), the most abundant, non-critical and less expensive rare-earth element, can be used as a dopant instead of Dy(III) for improving the properties of $Nd_2Fe_{14}B$ to some extent.[6] Research in the field of lighter rare-earth-based SIMs/SMMs that are comparatively more abundant in nature is still in the early stages.[7] This is due to the fact that the lighter lanthanide ions with less than half-filled f-orbitals have smaller magnetic momentum defined by $J = L–S$ and smaller spin–orbit (SO) coupling as compared to heavier lanthanides. Thus, it requires precise control of the ligand field and symmetry to realize SIM/SMM based on lighter lanthanides. Lately, few examples of lighter lanthanide-based SMMs have been reported in the literature.[7,8] Ce(III) being a single-electron system with oblate electronic density for the ground $m_J = \pm 5/2$ (ground electronic state $^2F_{5/2}$) provides a better understanding of the interplay of the ligand environment and symmetry in deciding magnetic anisotropy. Since the Ce(III) ion possesses only one unpaired electron ($4f^1$ configuration and $^2F_{5/2}$ as the ground state) and the natural isotopes of Ce(III) do not possess any nuclear spin, the manipulation of the electronic levels is easier compared to that for other ions and this has implication in the development of devices based on SMMs.[9] Earlier theoretical studies

[a]*Department of Chemistry, Indian Institute of Technology Bombay, Mumbai-400076, India. E-mail: rajaraman@chem.iitb.ac.in, rmv@chem.iitb.ac.in*
[b]*Department of Chemistry, SRM Institute of Science and Technology, Kattankulathur, Kancheepuram 603203, Tamil Nadu, India*
[c]*Physikalisches Institut, Karlsruhe Institute of Technology (KIT), Wolfgang-Gaede-Strasse 1, 76131 Karlsruhe; Institute of Nanotechnology, KIT, Hermann-von-Helmholz-Platz 1, 76344, Eggenstein-Leopoldshafen, Germany*

† Dedicated to Professor G. K. Lahiri on the occasion of his 60th birthday.

‡ Electronic supplementary information (ESI) available: Crystallographic details, magnetic studies and quantum mechanical calculations. CCDC 1590248 (**1**) and 1877236 (**2**). For ESI and crystallographic data in CIF or other electronic format see DOI: 10.1039/c9dt03052b

Table 1 Comparison of **1** with monometallic Ce(III), bimetallic Ce(III) and 3d-Ce(III)-based SMMs

Complex	U_{eff}/K	H_{dc}/Oe	Ground state KD	g_x, g_y, g_z	Ref.
1	21.5	200	0.54 |±1/2>, 0.24 |±5/2>, 0.22 |±3/2>	1.90, 1.67, 0.26	This work
$[Ce(NO_3)_3(18\text{-crown-}6)]$	31.4	1000	—	—	11*a*
$[Ce(NO_3)_3(1,10\text{-diaza-}18\text{-crown-}6)]$	44	1000	—	—	11*a*
$[Li(DME)_3][Ce(COT'')_2]$	30	400	|±1/2>	2.43, 2.36, 1.03	8*e*
$[Ce(dmso)_8][Ce(\eta_2\text{-}NO_3)_2(dmso)_4(\alpha\text{-}Mo_8O_{26})_{0.5}][Mo_6O_{19}]$	24.4	200	—	—	11*b*
$[Ce(NO_3)\{Zn(L^1)(SCN)\}_2]$	35.7	1000	—	—	11*c*
$[CeZn_2(L^1)_2(AcO)_2]BPh_4$	37	250			11*f*
$[Ce\{ZnI(L^2)\}_2(MeOH)]BPh_4$	21.2	0	0.78 |±5/2>, 0.10 |±3/2>	0.33, 0.48, 4.06	8*d* and 10*a*
$[CeCd_3(Hquinha)_3(n\text{-}Bu_3PO)_2I_3]\cdot 3EtOH\cdot 2H_2O$	27	1500	0.96|±3/2>	0.02, 0.10, 2.48	11*d*
$Ce(fdh)_3(bpy)$	33.3	2000	0.92|±5/2>	0.18, 0.46, 3.79	11*e*

18-Crown-6 = 1,4,7,10,13,16-hexaoxacyclooctadecane; 1,10-diaza-18-crown-6 = 1,4,10,13-tetraoxa-7,16-diazacyclooctadecane; DME = dimethoxyethane; COT'' = 1,4-bis(trimethylsilyl)cyclooctatetraenyldianion; dmso = dimethylsulfoxide; L^1 = 6,6′-(ethane-1,2-diylbis(azanylylidene)) bis(methanylylidene)bis(2-methoxyphenol); L^2 = 6,6′-(2,2-dimethylpropane-1,3-diyl)bis(azan-1-yl-1-ylidene)bis(methan-1-yl-1-ylidene) bis(2-methoxyphenol); H_2quinha = quinaldichydroxamic acid; fdh = 1,1,1-fluoro-5,5-dimethyl-hexa-2,4-dione; bpy = 2,2′-bipyridine.

highlight the importance of the ligand field around Ce(III) and some of the model system studies suggest that very strong axial ligation yields the largest theoretical barrier for fictitious $[Ce(OH)_2]^+$ models.[10]

While most of the reported Ce(III) complexes are field-induced SMMs,[8e,11] the only reported zero-field SMM based on Ce(III) is the linear trinuclear complex $[Ce\{ZnI(L^2)\}_2(MeOH)]BPh_4$ (see Table 1).[8d] In this complex, the zero-field SMM behaviour arises due to the presence of the Zn(II) ions near the axial sites, which increases the negative charge on the bridging phenoxy oxygen atoms ligated to the Ce(III) ion.[10a] In addition, the presence of zinc ions in the complexes invariably increases the net Ce(III)–Ce(III) distance in the lattice, weakening the dipolar interactions. In this work, we report a simple air-stable monometallic Ce(III) complex $[L_3Ce(NO_3)_3]$ (**1**) from a bulky phosphonic diamide ligand ^{t}BuPO(NH^{i}Pr)$_2$ (**L**),[12] that behaves as a single-ion single-electron magnet under a small applied magnetic field. In addition, we also present a cautionary note to the community citing the importance of the remnant magnetic field in SQUID magnetometers that can completely influence the interpretation of data in these systems. In order to explicate the novel magnetic properties displayed by Ce(III)-SIM, *ab initio* calculations based on CASSCF/RASSI-SO/SINGLE_ANISO have been performed, which underlines the important effect on the crystal field imparted by the phosphonic diamide ligands.

Experimental

Instruments and methods

Fourier-transform infrared spectra were recorded on a Perkin Elmer Spectrum One spectrometer using KBr diluted pellets. Elemental analyses were performed on a Thermoquest Flash EA 1112 series CHNS Elemental Analyzer. The magnetic properties were measured on the polycrystalline sample using Quantum Design MPMS-XL SQUID magnetometers equipped with a 7 T magnet in the temperature range of 2–300 K. The data were corrected for the background diamagnetic contribution and the diamagnetic contribution of the compounds was corrected using Pascal's constants. Alternating current (ac) susceptibility measurements were performed with an oscillating ac field of 3.5 Oe oscillating at indicated frequencies between 0.1 and 1500 Hz. The single-crystal measurements down to ultralow temperatures were performed on a micro-SQUID setup. The metal content in the diluted samples was measured by inductively coupled plasma atomic emission spectroscopy (ICP-AES) by digestion in nitric acid. Powder X-ray diffraction measurements were recorded on a Philips X'pert Pro (PANalytical) diffractometer using Cu Kα radiation (λ = 1.54190 Å).

Materials

Commercial grade solvents were purified by employing conventional procedures and distilled prior to use.[13] The phosphonic diamide ligand ^{t}BuPO(NH^{i}Pr)$_2$ (**L**) was synthesized using a previously reported procedure.[12] Cerium(III) nitrate hexahydrate and lanthanum nitrate hexahydrate were procured from Alfa Aesar and used as received.

Crystallography

Suitable single crystals of compounds **1** and **2** were mounted on a Rigaku Saturn 724+CCD diffractometer using Paratone oil for unit cell determination and three-dimensional intensity data collection. Data integration and indexing were carried out using CrystalClear and CrystalStructure.[14] The structures were solved using direct methods (SIR-97).[15] Structure refinement and geometrical calculations were carried out using programs in the WinGX module.[16] The final structure refinement was carried out using the full least square methods on F^2 using SHELXL-2014 (Table S1‡).[17] The structure refinement of compound **1** converged at R_1 = 0.0409, wR_2 = 0.0750, while that of compound **2** produced large residuals (R_1 = 0.1433, wR_2 = 0.2423). Attempts to obtain better X-ray diffraction data for this isomorphous lanthanum complex **2** were not successful. The purity and isomorphism of the bulk sample were, however, further confirmed by PXRD (*vide infra*).

Synthesis and characterization of $[\{^t$BuPO(NH^{i}Pr)$_2\}_3$Ce$(NO_3)_3]$ (1). To a solution of $Ce(NO_3)_3\cdot 6H_2O$ (108.6 mg, 0.25 mmol) in methanol (10 mL), a solution of ^{t}BuPO(NH^{i}Pr)$_2$ (165 mg, 0.75 mmol) in a mixture of acetonitrile and toluene

(15 mL) was added. The reaction mixture was stirred at 60 °C for 4 hours before cooling down to room temperature. The solution was then filtered and kept for crystallization at an ambient temperature. Crystals were obtained within a period of one to two weeks. Yield: 0.184 g (74.6%, based on ligand); Anal. Calcd for $C_{30}H_{75}CeN_9O_{12}P_3$: C, 36.51; H, 7.66; N, 12.77. Found: C, 36.63; H, 7.42; N, 12.98. FT-IR (KBr, cm^{-1}): 3358(s), 3261(m), 2970(s), 2905(w), 2871(m), 1465(br), 1442(s), 1422(s), 1384(vs), 1320(s), 1133(s), 1108(vs), 1055(s), 1022(s), 905(w), 881(w), 830(w), 654(m), 543(w), 513(w).

Synthesis and characterization of $[\{^t$BuPO(NH^{i}Pr)$_2\}_3$La$(NO_3)_3]$ (2). To a solution of $La(NO_3)_3{\cdot}6H_2O$ (108.25 mg, 0.25 mmol) in methanol (10 mL), a solution of ^{t}BuPO(NH^{i}Pr)$_2$ (165 mg, 0.75 mmol) in a mixture of acetonitrile and toluene (15 mL) was added. The reaction mixture was stirred at 60 °C for 4 hours before cooling it down to room temperature. The solution was then filtered and kept for crystallization at an ambient temperature. Crystals were obtained within a period of one to two weeks. Yield: 0.201 g (81.6%, based on ligand); Anal. Calcd for $C_{30}H_{75}LaN_9O_{12}P_3$: C, 36.55; H, 7.67; N, 12.79. Found: C, 36.74; H, 7.83; N, 12.56. FT-IR (KBr, cm^{-1}): 3358(s), 2968(vs), 2910(s), 2868(m), 1464(br), 1440(s), 1422(s), 1385(vs), 1368(m), 1309(vs), 1170(vs), 1134(vs), 1105(vs), 1050(s), 1022(m), 904(w), 881(s), 829(s), 653(m), 543(m), 514(m).

Synthesis and characterization of $[\{^t$BuPO(NH^{i}Pr)$_2\}_3$ $Ce_{0.29}La_{0.71}(NO_3)_3]$ (1@2). To a solution of $Ce(NO_3)_3{\cdot}6H_2O$ (27.15 mg, 0.0625 mmol) and $La(NO_3)_3{\cdot}6H_2O$ (81.19 mg, 0.1875 mmol) in methanol (10 mL), a solution of ^{t}BuPO(NH^{i}Pr)$_2$ (165 mg, 0.75 mmol) in a mixture of acetonitrile and toluene (15 mL) was added. The reaction mixture was stirred at 60 °C for 4 hours before cooling down to room temperature. The solution was then filtered and kept for crystallization at an ambient temperature. Crystals were obtained within a period of one to two weeks. Yield: 0.180 g (73.0%, based on ligand); Anal. Calcd for $C_{30}H_{75}Ce_{0.29}La_{0.71}N_9O_{12}P_3$: C, 36.74; H, 7.67; N, 12.78. Found: C, 36.63; H, 7.70; N, 12.2. FT-IR (KBr, cm^{-1}): 3356(s), 3336(s), 3263(m), 2966(s), 2908(s), 2869(m), 1464(br), 1442(s), 1397(vs), 1385(vs), 1320(s), 1170(s), 1133(s), 1108(vs), 1054(s), 1025(s), 1011(s), 904(m), 882(s), 830(m), 652(m), 638(w), 543(w), 513(w).

Computational details

Ab initio calculations were carried out on complex **1** to compute the *g*-tensors and the energies of the Kramers doublets. All the calculations were performed using MOLCAS 8.0 quantum chemistry package.[18] In this multi-configurational approach, the relativistic approach was treated based on Douglas–Kroll Hamiltonian. We employed atomic natural (ANO-RCC) basis set for the calculations of *g*-tensor. The following contraction schemes were employed: [8s7p5d3f2g1h] for Ce, [3s2p] for N, [4s3p2d1f] for O, [4s3p] for P, [3s2p] for C and [2s] for H. The ground state atomic multiplicity of Ce^{III} is $^2F_{5/2}$. The CASSCF calculation comprised an active space of one active electron in the seven active orbitals (CAS (1,7)). The CASSCF calculations were performed with 7 doublets. In the next step, we mixed these CASSCF computed spin-free states *via* the RASSI module to obtain the spin–orbit states. Here, we performed RASSI calculations with 7 doublet states and extracted the relative energies of Kramers doublets. In the last step, we used the SINGLE_ANISO code[19] implemented in MOLCAS to compute the *g*-tensors of Ce^{III} ion. Furthermore, our computed molar magnetic susceptibility and molar magnetization were computed and agreed reasonably (Fig. S1 and S2‡) with the experimental observations.

Results and discussion

Synthetic aspects and molecular structure

The bulky phosphonic diamide ligand ^{t}BuP(O)(NH^{i}Pr)$_2$ (**L**) was prepared according to a previously published method.[12] –P═O functionalities are known to provide stronger ligation to a metal ion, while the bulkier alkyl groups help in increasing the net metal–metal distance in the lattice, thereby reducing the intermolecular interactions. The $[L_3Ce(NO_3)_3]$ (**1**) and $[L_3La(NO_3)_3]$ (**2**) complexes were readily synthesized in high yields from the direct reactions of the ligand (**L**) and cerium nitrate hydrate and lanthanum nitrate hydrate, respectively, in a mixture of solvents, *viz.*, acetonitrile, methanol, and toluene (Scheme 1). Single crystals were obtained from the reaction mixture through the slow evaporation of the mother liquor and were characterized by both analytical methods and spectroscopic techniques. All compounds were perfectly stable in the presence of air or moisture for long periods. The FT-IR spectra of the compounds were recorded using KBr-diluted discs in the solid state. The IR spectra showed an absorption band at around 3300 cm^{-1}, corresponding to the presence of N–H stretching. The infrared absorptions observed in the

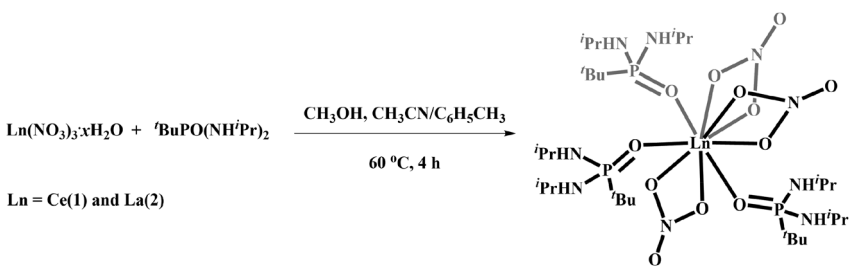

Scheme 1 Synthesis of monometallic Ln(III) complexes $[L_3Ln(NO_3)_3]$ [where Ln = Ce (**1**) and La(**2**)].

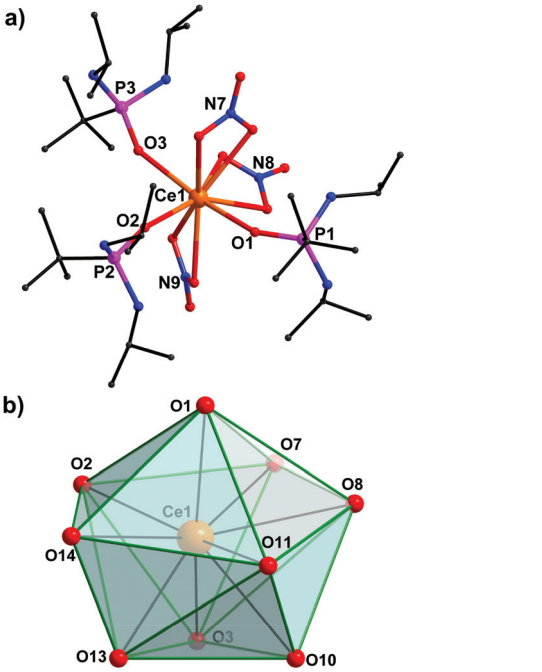

Fig. 1 (a) Molecular structure of **1** and (b) polyhedral view of the muffin-like coordination environment of Ce(III) ion in **1**.

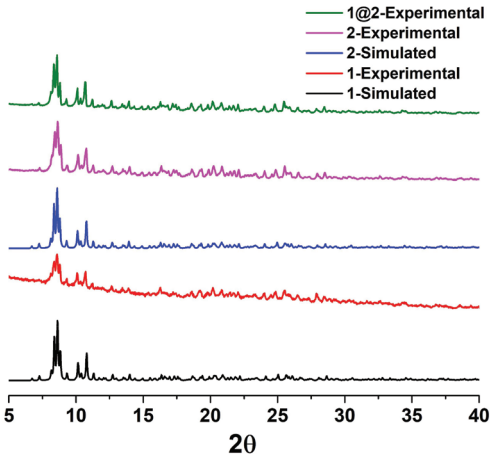

Fig. 2 Experimental and simulated PXRD profiles of the bulk samples for **1**, **2** and **1@2**.

2980–2850 cm^{-1} region were due to the presence of the aliphatic C–H vibrations originating from the phosphonamide ligand. The spectra further exhibited strong absorption around 1380 cm^{-1}, corresponding to the N–O vibrations of the nitrate anions. The characteristic P=O absorption was observed at around 1100 cm^{-1} for all the complexes.

Single crystal X-ray diffraction analysis revealed that compound **1** crystallized in the orthorhombic space group *Pbca* with the asymmetric part of the unit cell containing two chemically equivalent and crystallographically similar molecules. The Ce(III) ions occupied a nine-coordinate muffin-like coordination environment (Fig. 1 and Table S2‡). Six of these nine coordination sites were occupied by three chelating nitrate ligands and the remaining three sites were occupied by the phosphoryl oxygen atoms (Fig. 1). Three phosphonamide ligands coordinated to the central Ce(III) ion through phosphoryl oxygen in nearly T-shape geometry. Selected bond distances and bond angles are given in Table S3.‡ The average Ce1–O and Ce2–O distances were 2.536 and 2.548 Å, respectively. The average Ce–O(P) distance (2.377 Å) was much shorter than the average Ce–O(N) distance (2.625 Å). The nearest Ce(III)–Ce(III) distance in the lattice was 11.245 Å. The molecules in the asymmetric part were involved in intra- and intermolecular H-bonding interactions, leading to the formation of a complex three-dimensional network of mononuclear Ce(III) complexes in the 3D lattice (Fig. S3 and Table S4‡). The isomorphous lanthanum complex **2** displayed similar structural features. The average La–O(P) distance (2.406 Å) and the average La–O(N) distance (2.648 Å) in **2** were slightly longer as compared to those in **1** (it should be noted that the X-ray diffraction data for **2** were of poor quality). The phase purity of the samples was confirmed by the powder X-ray diffraction studies of the bulk samples in powder form (Fig. 2). The diluted sample **1@2** was prepared directly by crystallization from the reaction mixture.

Magnetic studies

The static magnetic properties of **1** were measured using polycrystalline powder samples in a temperature range of 2–300 K and in an applied field of 0.1 T. The $\chi_M T$ value of 0.67 cm^3 K mol^{-1} at 300 K was in good agreement with the calculated value of 0.81 cm^3 K mol^{-1} for an isolated Ce(III) ion (ground term symbol $^2F_{5/2}$, g = 6/7) (Fig. S1‡). The $\chi_M T$ value gradually decreased and reached 0.19 cm^3 K mol^{-1} at 2 K with the lowering of temperature due to the depopulation of the Stark levels split by the crystal field. The magnetization for **1** increased almost linearly up to 4 T before showing a gradual increase to reach a value of 0.62μ_B at 7 T although no saturation of magnetization was evident, further indicating the presence of significant anisotropy (Fig. S2‡).

In order to understand the relaxation dynamics, alternating current (ac) magnetic susceptibility measurements were recorded at zero dc field with an oscillating ac field of 3.5 Oe. Frequency-dependent maxima were observed in the out-of-phase magnetic susceptibility (χ'') component even at zero dc fields (Fig. S4c‡). It is interesting to note the presence of significant χ_s (adiabatic susceptibility) values at zero external dc field that corresponds to the faster spin–spin relaxation and is usually a result of dipolar interactions or the presence of the transverse components of magnetic anisotropy in a system (Fig. S4‡). A non-zero χ_s value has been observed in many Ce(III)-based SMMs (Table 1).[8d,e,11] This also suggested the presence of significant QTM in the ground state KD. A similar behaviour has also been observed in the case of zero-field SMM $[Ce\{ZnI(L^2)\}_2(MeOH)]BPh_4$.[8d] However, weak χ'' compared to χ' and high χ_s/χ_T (χ_s = adiabatic susceptibility and χ_T = isothermal susceptibility) prompted us to measure the ac mag-

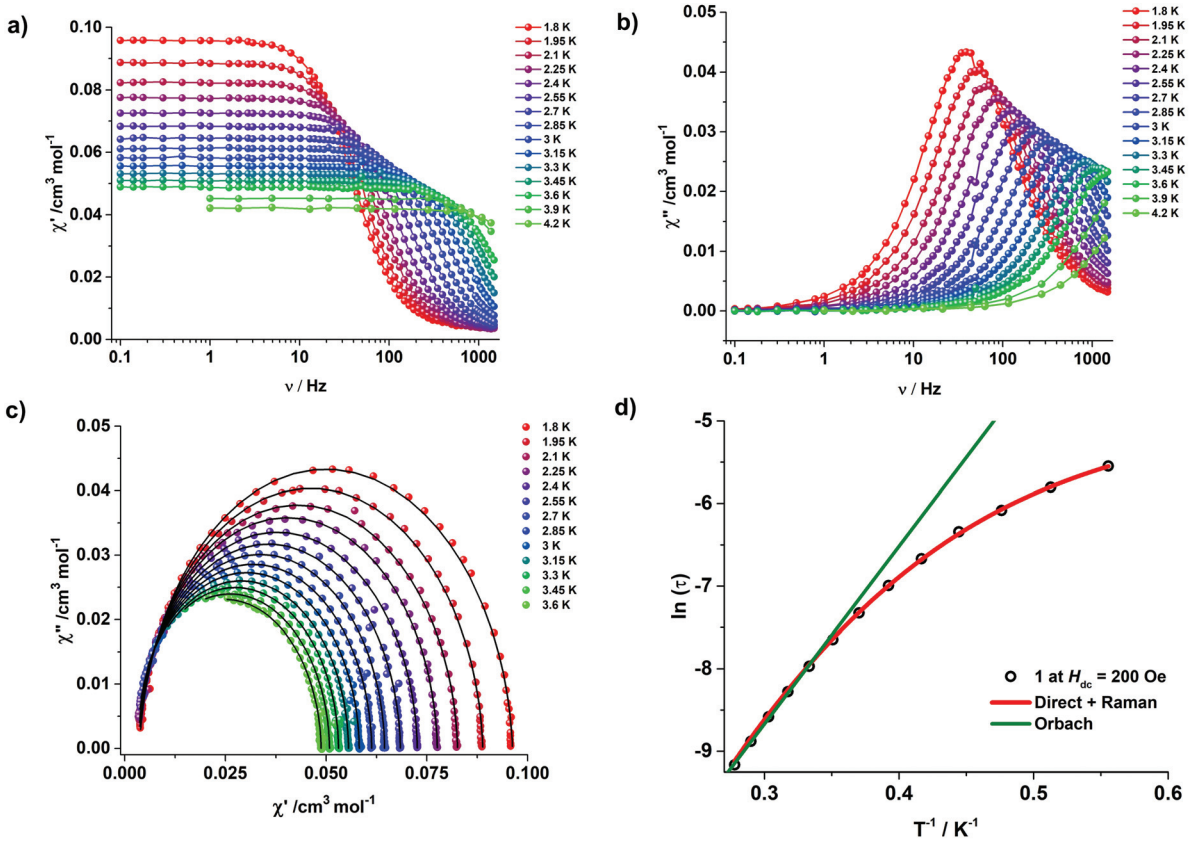

Fig. 3 (a) In-phase (χ'_M) and (b) out-of-phase (χ''_M) components of the frequency-dependent (0.1–1464 Hz) ac susceptibility in an oscillating ac field of 3.5 Oe under an applied dc field of 200 Oe for **1**. Solid lines are guides for the eyes. (c) Cole–Cole plot for **1** under an applied dc field of 200 Oe. Solid black lines are the best fit to the Debye model. (d) Plot of the relaxation time τ *versus* T^{-1} obtained for **1** under an applied dc field of 200 Oe. Solid lines are best fits to the multiple relaxation processes.

netic susceptibility at various fields at 1.8 K. It was surprising to note that the maxima in the out-of-phase signal disappeared at around 10 Oe, indicating the presence of a significant remnant field in MPMS. The remnant field measured with a standard Pd sample was found to be ~8.5 Oe (Fig. S4a‡). The maxima reappeared on increasing the dc field above 10 Oe. This observation indicated that the maxima in the out-of-phase signals at zero dc field were a result of the dc field offset in MPMS. This led us to measure the ac susceptibility of the sample in another MPMS, where the ac signals are more symmetric around zero field and maxima do not disappear on increasing the dc field (Fig. S5‡). The remnant field measured with the standard Pd sample was found to be ~2.0 Oe (Fig. S5‡). Hence, all further measurements were recorded on this system. From the variable field ac susceptibility measurements at 1.8 K, it was clear that there is significant tunnelling at zero dc field in **1** and the maxima in the first case were a result of the dc offset/remnant magnetic field in the system. However, a small dc field of even 10 Oe was enough to onset the suppressing of QTM in the system (Fig. S5‡). The ac susceptibility measurements were then recorded at an optimum dc field of 200 Oe. The application of an optimum dc field of 200 Oe resulted in the disappearance of χ_s with χ_s/χ_T (χ_T, the isothermal susceptibility refers to the spin–lattice relaxation) almost approaching zero at lower temperatures (Fig. 3). Frequency and temperature-dependent maxima were observed in the out-of-phase magnetic susceptibility (χ'') component up to 3.5 K (Fig. 3 and S6‡). The relaxation times (τ) were extracted from the frequency-dependent data using a generalized Debye model for a single relaxation process (Fig. 3). The α coefficients lie in a narrow range (0.018–0.042). The plot of the extracted $\ln(\tau)$ *vs.* T^{-1} (Fig. 3d) revealed a non-linear nature, indicating the presence of multiple relaxation processes. The best fit to the Arrhenius law near the higher temperatures estimated U_{eff} = 21.5 K and the pre-exponential factor as $\tau_0 = 2.7 \times 10^{-7}$ s. Since the anisotropic energy barrier was much lower than that estimated from the *ab initio* calculations (see below), this suggested that other relaxation pathways were operative. This was further supported by the analysis of the data considering the entire relaxation pathway as per the following equation:

$$\tau^{-1} = \frac{B_1}{1 + B_2 H^2} + AH^m T + CT^n + {\tau_0}^{-1} \exp\left(-\frac{U_{eff}}{k_B T}\right) \quad (1)$$

Here, the subsequent terms represent the contribution from QTM, direct, Raman and Orbach processes.[20] However,

attempts to extract the individual parameters for the QTM and direct process using the field-dependent relaxation time as per eqn (2) were unsuccessful.

$$\tau^{-1} = \frac{B_1}{1 + B_2 H^2} + AH^m T \quad (2)$$

The best fit to the relaxation time extracted from the frequency-dependent data could be obtained using the terms corresponding to the direct and Raman relaxation processes as per eqn (3) (Fig. 3d).

$$\tau^{-1} = DT + CT^n \quad (3)$$

Here, $D = AH^m$.

This resulted in D = 99.5 s^{-1} K^{-1}, C = 1.44 s^{-1} K^{-n} and n = 6.8. We assume that the application of an external dc field quenches QTM. Further fitting the relaxation time including the QTM term

$$\tau_{\mathrm{QTM}}{}^{-1} = \frac{B_1}{1 + B_2 H^2}$$

resulted in an insignificant value. This was also evident from the low-temperature measurements on a micro-SQUID setup, which showed that QTM is very prominent only at very low temperatures and the molecules relax *via* a direct process under dc fields at higher temperatures (see below). In order to gain further insights into the relaxation dynamics, we also prepared a 29.0% (±0.2) diluted sample of **1** (**1@2**) in an isomorphous diamagnetic lanthanum complex $[L_3La(NO_3)_3]$ (**2**) and relatively decent ac susceptibility data could be obtained (Fig. S7 and S8‡). A relatively lower dc field was required to quench QTM. The ac susceptibility measurements were recorded under an optimum field of 30 Oe and similar relaxation dynamics were observed for the diluted sample with the frequency and temperature-dependent maxima observed in the out-of-phase magnetic susceptibility (χ'') component up to 3.5 K (Fig. S8‡). In order to gain further insights, we carried out low-temperature magnetic measurements on a micro-SQUID setup with the oriented crystals of **1**. The low-temperature measurements on a micro-SQUID setup were performed with oriented crystals of **1** aligned with the transverse field method.[21] At the lowest measurement temperature of 30 mK and at higher field sweep rates, significant QTM was present as the tunnelling rates were faster than the time scale of the applied field sweep rates (Fig. 4). The molecules that do not reverse their spin at the zero-field step relax *via* a direct relaxation process at higher fields. At intermediate and lower field sweep rates, there is also evidence for a phonon-bottleneck process.[22] At the lowest field sweep rates and at the lowest temperature, due to the population of the excited state, fewer molecules underwent quantum tunnelling of magnetization and hence, the corresponding step at zero field was smaller. Upon increasing the temperature at which the measurements were done, there was again less QTM due to the population of the excited state (Fig. S9‡). Upon a further temperature increase, the sample behaved like a paramagnet, the remaining slight opening of the loops being due to a phonon bottleneck (Fig. S11‡). Overall, the hysteresis loops showed temperature and field sweep-rate dependence, with the coercivity increasing on increasing the field sweep rates and decreasing the temperature, confirming the SIM behaviour of complex **1**. The strong tunnelling observed at zero-field was consistent with the theoretical results (please see next section), where strong mixing of the ground state with higher excited m_J levels was detected.

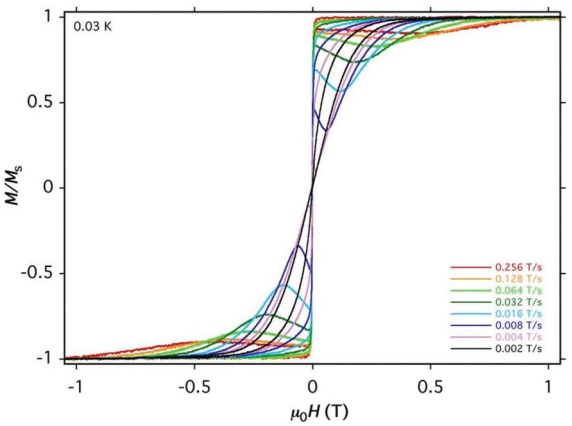

Fig. 4 Normalized field-dependent magnetization data performed with the oriented crystals of **1**, aligned with the transverse field method at 30 mK with varying field sweep rates.

Electronic structure calculations

In order to obtain insights about the electronic structure of **1**, we carried out *ab initio* calculations (CASSCF/RASSI/SANISO) on the X-ray structure (see computational details). The analysis of the *g*-tensors of ground state Kramers doublet (KD) showed that the equatorial terms (g_{xx}, g_{yy}) were larger in magnitude compared to the axial (g_{zz}) term, showing the existence of transverse anisotropy (Table S10‡). The wavefunction analysis illustrated the stabilization of mixed m_J levels (Tables S10 and S11‡). Also, g_{zz} was oriented closer to one of the oxygen atoms of phosphonic diamide ligands (deviated by 38.1° from the oxygen atom). The analysis of the CASSCF computed LoProp charges (Table S12‡) showed larger negative charges on the phosphonic diamide oxygen atoms compared to that on the nitrate oxygens, thus dictating the orientation of g_{zz} to a larger extent. The computation of the transverse magnetic moments connecting the opposite pairs of magnetization showed the existence of QTM in the mechanism of relaxation, which was in line with the observation of the mixed m_J values in the ground state KD as well as the experimental fit. The first excited state was found to lie at 220 cm^{-1} and the angle between g_{zz} of the ground state and the first excited state was large, suggesting relaxation *via* the first excited state considering only the Orbach process. The large difference between the computed energy barrier (Orbach process) and the fitted values clearly showed the possibility of other relaxation mechanisms involving a direct/Raman process or intermolecular

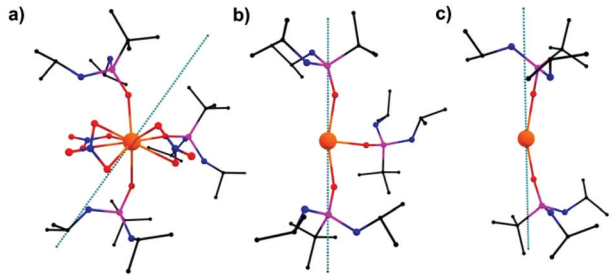

Fig. 5 CASSCF-computed g_{zz} orientation of the ground state KD of complexes (a) **1**, (b) **1a** and (c) **1b**.

interactions, which were found to play a crucial role in previous lighter lanthanide studies;[8a,10,11e] these are not included in our current calculations. A short Ce(III)–Ce(III) distance in the lattice also suggested that to some extent, intermolecular interactions might quench the ground state QTM effect, leading to the observation of SIMs with a relatively smaller U_{eff} value.

We also calculated the *g*-tensors and effective barrier for the other chemically equivalent complex in the unit cell (**1′**) and the magnetic properties of this complex also resembled those of complex **1** with slight difference owing to the variance in their structures (Tables S10, S12, and S13‡). To find ways to quench the QTM observed in the ground state KDs and to obtain insights in the role of phosphonic diamide ligands, we carved three-coordinate ($[L_3Ce]^{3-}$, **1a**) and two coordinate ($[L_2Ce]^{3-}$, **1b**) models (Fig. 5b and c) out of complex **1** and the following observations could be made from these calculations on **1a** and **1b**: (a) the magnitude of the g_{zz} tensor increased considerably compared to that for **1** with negligible transverse anisotropy terms, providing a strong axial character and Ising nature to the ground state KDs of **1a** and **1b**, respectively (Table S10‡). (b) The orientation of g_{zz} (Fig. 5b and c) moved closer to the oxygen atom of phosphonic diamide and the angles between g_{zz} of ground state and excited KDs decreased, resulting in relaxation *via* higher excited states (U_{cal} = 627 cm^{-1} (**1a**), 2394 cm^{-1} (**1b**), Table S10‡). As the coordination number decreased, the quenching of QTM was accompanied by the stabilization of higher m_J levels (Tables S14 and S15‡) in the ground state, leading to the realization of relaxation *via* higher excited states and larger barrier heights.

Conclusions

In summary, a carefully chosen ligand field around Ce(III) led to the isolation of a single-ion single-electron magnet, which exhibited slow relaxation dynamics under an applied dc field. The metal ion in SIM was present in muffin-like coordination geometry. Both dynamic ac susceptibility measurements and low-temperature hysteresis measurements on a micro-SQUID setup with oriented crystals revealed that in **1**, relaxation proceeded *via* direct and Raman processes. *Ab initio* calculations revealed the stabilization of the mixed m_J levels in the ground state with significant tunnelling probability, but the first excited state was found to be higher in energy due to significantly different charge distribution in the axial and equatorial oxygen atoms. Furthermore, ways to quench the QTM in Ce-SIMs were illustrated by using low coordinate models. Efforts to synthesize low coordinate cerium complexes in order to enhance the effective energy barrier is currently underway in our laboratory.

Conflicts of interest

There are no conflicts to declare.

Acknowledgements

This work was supported by a SERB J. C. Bose National Fellowship to RM (SB/S2/JCB-85/2014). GR thanks SERB (CRG/2018/000430) and UGC-UKIERI (184-1/2018(IC)) for the financial support. We acknowledge Dr L. Ungur and Prof. L. F. Chibotaru, Belgium for additional MOLCAS routines. SKG and AB thank DST-SERB and UGC New Delhi for research fellowships, respectively.

Notes and references

1 (*a*) M. Mannini, F. Pineider, P. Sainctavit, C. Danieli, E. Otero, C. Sciancalepore, A. M. Talarico, M.-A. Arrio, A. Cornia, D. Gatteschi and R. Sessoli, *Nat. Mater.*, 2009, **8**, 194–197; (*b*) M. Urdampilleta, S. Klyatskaya, J. P. Cleuziou, M. Ruben and W. Wernsdorfer, *Nat. Mater.*, 2011, **10**, 502–506; (*c*) S. G. McAdams, A.-M. Ariciu, A. K. Kostopoulos, J. P. S. Walsh and F. Tuna, *Coord. Chem. Rev.*, 2017, **346**, 216–239.

2 N. Ishikawa, M. Sugita, T. Ishikawa, S.-y. Koshihara and Y. Kaizu, *J. Am. Chem. Soc.*, 2003, **125**, 8694–8695.

3 (*a*) D. N. Woodruff, R. E. P. Winpenny and R. A. Layfield, *Chem. Rev.*, 2013, **113**, 5110–5148; (*b*) L. Sorace, C. Benelli and D. Gatteschi, *Chem. Soc. Rev.*, 2011, **40**, 3092–3104; (*c*) C. A. P. Goodwin, F. Ortu, D. Reta, N. F. Chilton and D. P. Mills, *Nature*, 2017, **548**, 439–442; (*d*) S. K. Gupta, T. Rajeshkumar, G. Rajaraman and R. Murugavel, *Chem. Sci.*, 2016, **7**, 5181–5191; (*e*) F.-S. Guo, B. M. Day, Y.-C. Chen, M.-L. Tong, A. Mansikkamäki and R. A. Layfield, *Angew. Chem., Int. Ed.*, 2017, **56**, 11445–11449; (*f*) R. J. Blagg, L. Ungur, F. Tuna, J. Speak, P. Comar, D. Collison, W. Wernsdorfer, E. J. L. McInnes, L. F. Chibotaru and R. E. P. Winpenny, *Nat. Chem.*, 2013, **5**, 673–678; (*g*) K. R. Meihaus and J. R. Long, *J. Am. Chem. Soc.*, 2013, **135**, 17952–17957; (*h*) J. J. Le Roy, L. Ungur, I. Korobkov, L. F. Chibotaru and M. Murugesu, *J. Am. Chem. Soc.*, 2014, **136**, 8003–8010; (*i*) J. D. Rinehart, M. Fang, W. J. Evans and J. R. Long, *J. Am. Chem. Soc.*, 2011, **133**, 14236–14239; (*j*) S. K. Gupta, T. Rajeshkumar, G. Rajaraman and R. Murugavel, *Dalton Trans.*, 2018, **47**, 357–366.

4 J. D. Rinehart and J. R. Long, *Chem. Sci.*, 2011, **2**, 2078–2085.
5 (*a*) Y. Li, X. L. Zhang, R. Qiu and Y. S. Kang, *Colloids Surf., A*, 2008, **313–314**, 621–624; (*b*) P. K. Deheri, V. Swaminathan, S. D. Bhame, Z. Liu and R. V. Ramanujan, *Chem. Mater.*, 2010, **22**, 6509–6517.
6 A. K. Pathak, M. Khan, K. A. Gschneidner, R. W. McCallum, L. Zhou, K. Sun, K. W. Dennis, C. Zhou, F. E. Pinkerton, M. J. Kramer and V. K. Pecharsky, *Adv. Mater.*, 2015, **27**, 2663–2667.
7 F. Pointillart, O. Cador, B. Le Guennic and L. Ouahab, *Coord. Chem. Rev.*, 2017, **346**, 150–175.
8 (*a*) S. K. Gupta, T. Rajeshkumar, G. Rajaraman and R. Murugavel, *Chem. Commun.*, 2016, **52**, 7168–7171; (*b*) J. D. Rinehart and J. R. Long, *Dalton Trans.*, 2012, **41**, 13572–13574; (*c*) J. J. Le Roy, S. I. Gorelsky, I. Korobkov and M. Murugesu, *Organometallics*, 2015, **34**, 1415–1418; (*d*) S. Hino, M. Maeda, K. Yamashita, Y. Kataoka, M. Nakano, T. Yamamura, H. Nojiri, M. Kofu, O. Yamamuro and T. Kajiwara, *Dalton Trans.*, 2013, **42**, 2683–2686; (*e*) J. J. Le Roy, I. Korobkov, J. E. Kim, E. J. Schelter and M. Murugesu, *Dalton Trans.*, 2014, **43**, 2737–2740.
9 L. Bogani and W. Wernsdorfer, *Nat. Mater.*, 2008, **7**, 179.
10 (*a*) S. K. Singh, T. Gupta, L. Ungur and G. Rajaraman, *Chem. – Eur. J.*, 2015, **21**, 13812–13819; (*b*) T. Gupta and G. Rajaraman, *J. Chem. Sci.*, 2014, **126**, 1569–1579.
11 (*a*) H. Wada, S. Ooka, T. Yamamura and T. Kajiwara, *Inorg. Chem.*, 2017, **56**, 147–155; (*b*) A. B. Khelifa, M. S. Belkhiria, G. Huang, S. Freslon, O. Guillou and K. Bernot, *Dalton Trans.*, 2015, **44**, 16458–16464; (*c*) C. Takehara, P. L. Then, Y. Kataoka, M. Nakano, T. Yamamura and T. Kajiwara, *Dalton Trans.*, 2015, **44**, 18276–18283; (*d*) Q.-W. Li, R.-C. Wan, Y.-C. Chen, J.-L. Liu, L.-F. Wang, J.-H. Jia, N. F. Chilton and M.-L. Tong, *Chem. Commun.*, 2016, **52**, 13365–13368; (*e*) M.-X. Xu, Y.-S. Meng, J. Xiong, B.-W. Wang, S.-D. Jiang and S. Gao, *Dalton Trans.*, 2018, **47**, 1966–1971; (*f*) H. Shiori, M. Moe, K. Yumiko, N. Motohiro, Y. Tomoo and K. Takashi, *Chem. Lett.*, 2013, **42**, 1276–1278.
12 R. Murugavel and R. Pothiraja, *New J. Chem.*, 2003, **27**, 968–974.
13 W. L. F. Armarego, *Purification of laboratory chemicals/W.L.F. Armarego and D.D. Perrin*, Butterworth Heinemann, Oxford, Boston, 1996.
14 *CrystalClear, Version-SM Expert 2.0 r4, 2009 and CrystalStructure, Version 4.0*, Rigaku, Rigaku Americas and Rigaku, The Woodlands, Texas, USA, 2010 and Rigaku Corporation, Tokyo, Japan.
15 A. Altomare, M. C. Burla, M. Camalli, G. L. Cascarano, C. Giacovazzo, A. Guagliardi, A. G. G. Moliterni, G. Polidori and R. Spagna, *J. Appl. Crystallogr.*, 1999, **32**, 115–119.
16 L. Farrugia, *J. Appl. Crystallogr.*, 2012, **45**, 849–854.
17 G. Sheldrick, *Acta Crystallogr., Sect. C: Struct. Chem.*, 2015, **71**, 3–8.
18 (*a*) F. Aquilante, L. De Vico, N. Ferré, G. Ghigo, P.-å. Malmqvist, P. Neogrády, T. B. Pedersen, M. Pitoňák, M. Reiher, B. O. Roos, L. Serrano-Andrés, M. Urban, V. Veryazov and R. Lindh, *J. Comput. Chem.*, 2010, **31**, 224–247; (*b*) J. A. Duncan, *J. Am. Chem. Soc.*, 2009, **131**, 2416–2416; (*c*) V. Veryazov, P.-O. Widmark, L. Serrano-Andrés, R. Lindh and B. O. Roos, *Int. J. Quantum Chem.*, 2004, **100**, 626–635; (*d*) G. Karlström, R. Lindh, P.-Å. Malmqvist, B. O. Roos, U. Ryde, V. Veryazov, P.-O. Widmark, M. Cossi, B. Schimmelpfennig, P. Neogrady and L. Seijo, *Comput. Mater. Sci.*, 2003, **28**, 222–239.
19 L. Chibotaru and L. Ungur, *The computer programs SINGLE_ANISO and POLY_ANISO*, University of Leuven, 2006.
20 E. Lucaccini, L. Sorace, M. Perfetti, J.-P. Costes and R. Sessoli, *Chem. Commun.*, 2014, **50**, 1648–1651.
21 W. Wernsdorfer, N. E. Chakov and G. Christou, *Phys. Rev. B: Condens. Matter Mater. Phys.*, 2004, **70**, 132413.
22 I. Chiorescu, W. Wernsdorfer, A. Müller, S. Miyashita and B. Barbara, *Phys. Rev. B: Condens. Matter Mater. Phys.*, 2003, **67**, 020402.